Case Studies in Construction Materials 17 (2022) e01400

Contents lists available at ScienceDirect

Case Studies in Construction Materials

journal homepage: www.elsevier.com/locate/cscm

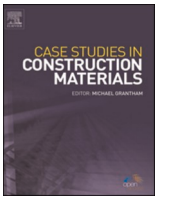

An experimental investigation on tensile behaviour of corroded ultra-high-performance concrete

Iftekhair Ibnul Bashar, Phillip Visintin *, Abdul Hamid Sheikh

School of Civil, Environmental & Mining Engineering, The University of Adelaide, SA 5005, Australia

ARTICLE INFO

Keywords:
Ultra-high-performance concrete
Fibre reinforced concrete
Corrosion
Direct tensile test

ABSTRACT

When UHPFRC is exposed to a corrosive environment, steel fibres may undergo corrosion which may affect the interfacial bond and therefore the overall tensile behaviour of UHPFRC. Previous studies have predominately investigated the influence of fibre corrosion on the tensile behaviour of UHPFRC using the flexural test method. In this approach, the significant variation in crack width may lead to variation in the level of corrosion, making it more difficult to develop material models. In this study, the influence of corrosion on the tensile resistance of UHPFRC has been studied using direct tensile test of thirty-nine grooved prisms with a range of different pre-cracking conditions and corrosion levels. The results show that even when crack widths are large, fibre corrosion has a relatively minor impact on the tensile performance of UHPFRC, and the expected level of deterioration is reduced due to self-healing of cracks and continued hydration of the cement when immersed in the chloride solution. When uncracked specimens are subjected to corrosive environments it was shown that the tensile strength was significantly increased due to enhanced hydration of the binder and associated pozzolanic reaction with silica fume. Despite the degree of experimental scatter and the competing mechanisms of corrosion and self-healing, the residual response of the corroded specimens has been found similar to that of the control specimens.

1. Introduction

Ultra-high-performance fibre reinforced concrete (UHPFRC) is increasingly being applied in scenarios where its post-cracking tensile strength and ductility are beneficial [1,2]. One of the major benefits of fibre reinforcement is the ability to simplify the detailing of traditional reinforcement by reducing reinforcement ratios and instead relying partially on the contribution of the fibres to transfer stresses across cracked planes [3]. While this approach has significant potential construction benefits, the experimental findings that support it are typically obtained from instantaneous testing of members constructed shortly before testing, and which have not been subjected to any environmental conditioning or previous loading. The consequence of this testing approach is that an upper-bound estimate of the contribution of fibres to overall member performance is obtained. That is, outside of the lab, the performance of members may be significantly influenced by time (shrinkage), sustained loading and load history (creep and fatigue), environmental conditioning (corrosion), and the coupling of all of the above [4,5]. Although it is expected that the application of fibre reinforced concrete will be beneficial even in scenarios where the potential for corrosion is high, because of a lack of material models to quantify long-term performance, current design standards do not allow the beneficial effects of fibres to be considered [6,7]. It is

* Corresponding author.
E-mail address: phillip.visintin@adelaide.edu.au (P. Visintin).

https://doi.org/10.1016/j.cscm.2022.e01400
Received 8 June 2022; Received in revised form 26 July 2022; Accepted 11 August 2022
Available online 13 August 2022

therefore the purpose of this work to assess the impact of fibre corrosion on the tensile stress/crack-width (σ/w) behaviour of UHPFRC. Significantly, this work specifically considers members with large crack widths such that an upper-bound to the expected damage from corrosion can be identified.

Numerous studies have been conducted to quantify the corrosion resistance of steel fibre reinforced concretes (SFRC) [e.g., [8–10]]. To assist in the design of the experimental work contained in this paper, and to provide guidance for future studies, a statistical overview of 342 individual test results obtained from 20 studies [8,10–28] is contained in the associated Data-in-Brief article. This overview shows that tests to quantify the impact of corrosion have considered a relatively narrow range of compressive strengths (typically either 60–70 MPa or greater than 150 MPa) and with up to 2 % fibre content. Also of significance, it is shown that only 29 % of the tests identified considered concrete that had been cracked prior to immersion in a corrosive substance. This is important, because the presence of cracks provide a pathway for more rapid chloride ingress and hence without pre-cracking a lower-bound estimate of durability may be obtained.

Regardless of the material type, the review of previous testing shows that extracting the influence/ level of corrosion on material properties of fibre reinforced concrete challenging. This is because the variation in material properties that occur because of fibre corrosion are similar in magnitude to the natural variation in properties that occur due to local variations in local fibre volume fractions and orientations. Additionally, the small physical size of a fibre makes it difficult to measure the degree of corrosion directly, and leads to the application of indirect measures such as simple observations of surface colour change [11] or the measurement of electric potential [12].

In previous research it has also been common (70 % of the test database) to conduct flexural or split tensile tests and apply inverse analysis techniques to infer the tensile stress/strain (σ/ε) and stress/crack-width σ/w behaviour [13]. This is important because when using flexural tests, a variation in crack opening along the height of a specimen occurs, and therefore, at each height along the crack there is a different level of damage prior to the commencement of conditioning to induce corrosion. Hence when applying inverse analysis techniques to extract the material σ/w from the experimental observations, an additional level of complexity and uncertainty is introduced because the level of corrosion can be expected to be influenced by the level of crack opening and damage prior to corrosion [14,15]. As an alternative to flexural tensile test methods, a significantly smaller number of studies have been conducted using direct-tension test specimens [10,16–18]. While the direct-tension test specimen cannot entirely remove variations in crack width which will occur due to the local variation in fibre density and material properties, this test method does minimise it. In addition, the direct-tension approach does not require the inference of material properties using inverse analysis, but rather utilises direct measurement to provide the elastic modulus, σ-w relationship, and tensile strength [29] while also minimising statistical uncertainty.

When considering previous direct tensile tests, Yoo et al. [18] used dog-bone shaped specimens made of UHPFRC containing of 2 % pre-corroded washed and unwashed macro steel fibres. A challenge with this work is that the method of corrosion (pre-corroding) yields and upper bound estimate of the impact of material properties because it does not allow for any protection that is provided by the concrete of the fibres and therefore any influence of the spatial variation of fibre corrosion. A further challenge with the work of both Tran et al. [10], Yoo et al. [16,17], and Yoo et al. [19] is that the results have been obtained from specimens that have thicknesses

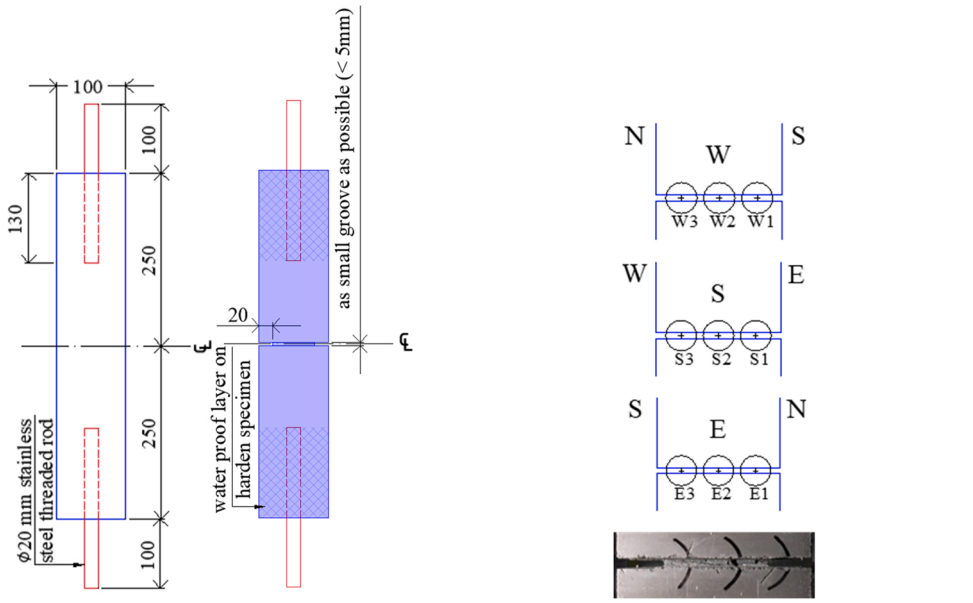

Fig. 1. Test specimen geometry and location for crack-width measurement with microscope.

less than the fibre length. This has a significant effect on specimen response because the small thickness of specimens restricts the fibres to alignment in a specific loading plane, which provides higher strength than expected in elements of the size common in practice [30, 31].

To address the above issues, in this work, the tensile response of UHPFRC at a lower strength range is quantified. To minimise uncertainty that arises from processing of test results, a direct tensile test approach is used where crack-widths are measured at various locations along a predefined plane where cracking is either not induced prior to inducing corrosion, or cracking is induced to either a 'low' or 'high' degree. To avoid any potential improvement in σ/w that may arise from specimen size, a specimen cross section that is more than 7 times the length of the fibre is used.

In the remainder of the paper, the design of the test specimens is first explained, this is followed by a description of the test methodology and conditioning regime. The test results are then presented along with a discussion of the change specimen strength and σ/w behaviour.

2. Materials and methods

To investigate the impact of fibre corrosion on the tensile response of UHPFRC, 39 direct-tension tests were conducted. The specimens were prismatic in geometry with a 100 mm × 100 mm cross-section and a length of 500 mm (Fig. 1(a)). To facilitate the direct-tension test, 230 mm long threaded stainless-steel bars (20 mm diameter) were cast along the specimen longitudinal axis at its two ends with an embedment length of 130 mm (Fig. 1(a)). The embedment length of the reinforcement was based on bond strength properties quantified by [32] and which were used as the basis of the test specimen design of [33], who used a similar setup and concrete mix design to test high-cycle fatigue properties and did not observe pull-out of the bars.

After curing, a 20 mm deep and 4 mm wide groove was cut into all specimens at the length to ensure crack development at this grooved plane. To further help avoid any possible corrosion of the threaded bars at their embedded interfaces, the external surface of the specimens near the ends were covered with a wax water proofing layer before immersion.

Table 1 provides the details of the test specimens, which can be categorised by their degree of pre-cracking: either uncracked or pre-cracked to a 'low' or 'high' degree. The degree of cracking was defined in earlier studies based on either crack opening, or strain measurements, however, in this study, the level of cracking is determined based on the sections post-cracking load resistance. The 'low' degree of cracking has been defined as a 15 % reduction in the ultimate load after cracking and 'high' degree of cracking has been defined as a 30 % reduction in the ultimate load after cracking. The decision to base the degree of cracking on a level of reduction in load was taken to reflect the random variation that occurs in UHPFRC stress crack-width behaviour, and the way this translates to variations in crack-width at the member level. That is, within a constant moment region of a beam, there will be a significant variation in crack-width that occurs because of the local variation in fibre content and orientation.

The specimens subjected to corrosion were immersed in sodium chloride solution for either 4, 12, 24 weeks, and the results compared to a control group which were aged under ambient lab conditions. A detailed breakdown of all test specimens is provided in Table 1, where each specimen is designated according to the initial crack-width before immersion, followed by the immersion length. For example, specimen cw15-imm24 has been pre-cracked until the load reduced by 15 % from the ultimate load, the specimen is then immersed for 24 weeks prior to testing. For specimens not subjected to any immersion an additional designation is used to identify the age at testing. For example, cw0-imm0w-223d refers to a specimen with no pre-cracking that has not been immersed and that has been tested at an age of 223 days.

2.1. UHPFRC mix design and casting

All specimens have been manufactured using a UHPFRC mix design developed at the University of Adelaide and previously reported in Sturm et al. [34], the proportion of individual constituents with respect to unit cement weight is given in Table 2.

Table 1
Specimen designation and test conditions.

Specimen designation	Age form		Pre-crack condition	Cl^- immersion condition	Number of specimens
	Cl^- immersion (weeks)	casting (days)			
cw0-imm0w-30d	0	30	uncracked	Not immersed	3
cw0-imm0w-80d	0	80			3
cw0-imm0w-139d	0	139			3
cw0-imm0w-223d	0	223			3
cw0-imm4w	4	80	uncracked	Immersed	3
cw0-imm12w	12	139			3
cw0-imm24w	24	223			3
cw15-imm4w	4	80	Pre-cracked (low - 15 %)	Immersed	3
cw15-imm12w	12	139			3
cw15-imm24w	24	223			3
cw30-imm4w	4	80	Pre-cracked (high - 30 %)	Immersed	3
cw30-imm12w	12	139			3
cw30-imm24w	24	223			3

The mix design in Table 2 was batched using a sulphate resisting cement and silica fume as a binder and a mined sand with a maximum particle size of 4.75 mm as a filler. When batching the concrete, the cement and silica fume were placed in a pan mixer which was run for 3 min to combine the binders, the sand was then added, and the mixer was run for a further 5 min. A blend of water and the high range water reducer (Sika ViscoCrete 10 HWRRe) was then slowly added, and mixing continued until a uniform flowable mortar was observed (approximately 15 min after the addition of the liquid components). Once flowable, the straight copper coated steel micro fibres, which had a diameter of 0.2 mm, and a length of 13 mm were added. Mixing was continued until the fibres were observed to be uniformly incorporated, this process took approximately three minutes.

The fresh UHPFRC was then cast (Fig. 2(d)), and once the concrete was finished, all specimens were kept moist under wet hessian in ambient lab conditions until they were demoulded at an age of 7 days. Once demoulded all specimens were stored in a temperature and humidity-controlled room (20 °C and 50 % humidity) until the time of testing.

2.2. Specimen pre-cracking

Specimens were pre-cracked by applying a displacement controlled tensile load through the stainless-steel bars using an INSTRON universal testing machine (UTM). Specimens were loaded under displacement control at a rate of 0.1 mm/min until the post-cracking load dropped by either 15 % or 30 % of the ultimate load for low pre-cracking and high pre-cracking specimens, respectively. Once the target load level was reached, the UTM was paused and the applied load held until the initial crack-width was measured at 9 (3 × 3) locations along the cracked plane (one side, which was the top exposed surface of the moulds, was excluded due to its unevenness). Specimens were then fully unloaded at a rate of 0.1 mm/min and the top grip (moving jaw) of the INSTRON released before measuring the residual crack-width at the same locations. In addition to the measurement of crack-width using a hand-held microscope, four 10 mm LVDTs (located at the four corners of specimens) measured the crack opening over a gauge length of 33.5 mm (Fig. 3). Upon completion of pre-cracking and residual crack-width measurement, the specimens were carefully removed from the UTM and immersed induce corrosion.

2.3. Specimen preconditioning and testing

To accelerate corrosion of fibres, specimens were immersed in a sodium chloride solution of 3%w.t. concentration (3 gm NaCl per 100 ml solution). A reservoir with a volume approximately 25 times of the volume of the specimens was used to immerse 6 specimens at a time. The specimens were placed horizontally resting on two timber blocks at the two sides of the vertical cracked plane so that chloride solution could freely flow near the cracked region to induce corrosion. For the first twelve weeks of immersion the chloride solution was changed at four-week intervals, after which point it was changed at six-week intervals.

At the day of testing, the specimens were removed from the reservoir and cleaned with fresh tap water to enable clear measurement of crack-width. Before placing the specimens in the UTM, the initial crack-width was remeasured at all nine predefined measurement locations using a microscope. The specimen was reinstalled in the UTM the four LVDTs were reinstalled for measuring crack-width at the four specimen corners (Fig. 3). During testing, the tensile load is again applied to maintain a displacement rate of 0.1 mm/min up to 2.5 mm displacement followed by 0.4 mm/min until the end of testing.

3. Results and discussions

The average 28-day compressive strength of the UHPFRC, obtained by testing 3 cylinders with a diameter of 100 mm and a height of 200 mm, was 125 MPa. The measured direct-tensile load (P) and crack-width (w) test data obtained from all tensile test specimens is provided in Supplementary Material S1. To allow for replicate tests, each test is designated with an additional modifier to identify replicate number. For example, cw15-imm4–2 indicates the second (−2) specimen that has been elongated beyond the peak load up to displacement to have 15 % reduction of peak load (cw15) for pre-cracking and the specimen has been immersed in chloride solution for 4 weeks (imm4) after pre-cracking.

In this section, the tensile load (P) has been converted to a tensile stress (σ) by dividing P by the minimum cross-sectional area (60 × 60 mm^2) of the specimen at the groove. The crack width (w) is taken as the average readings of the four LVDTs (one located at each corner of the specimen measuring over a gauge length of 33.5 mm).

3.1. Stress-crack width (σ-w) response of uncracked specimens

3.1.1. Un-corroded specimens

First let us consider the behaviour of the uncorroded specimens that were not subjected to any pre-cracking, such that it is possible

Table 2
UHPFRC mix design in proportion to unit weight of cement [34].

Cement (Sulphate resisting)	Silica fume	Mined sand (≤ 4.75 mm)	Water	Super plasticizer (Sika ViscoCrete 10 HWRRe)	Straight steel micro fibre[a]
1	0.266	1	0.19	0.045	0.165[a]

[a] 2% volume fraction (Ø 0.2 diameter × 13 mm length)

(a) Before fibre addition (b) After fibre addition but not mixed together

(c) UHPFRC mix in final stage

(d) Moulds for direct-tension test specimens (e) Casting of specimens

Fig. 2. Mixing of UHPFRC and casting of specimens.

to determine the influence of specimen aging on the corresponding stress crack-width (σ/w) behaviour. The average tensile stress and crack-width of cw0-imm0 specimens at age 28-, 80-, 139- and 223-days are shown in Fig. 4, in which the full σ/w response is given in part (a) and the initial 0.2 mm showing strain hardening is given in part (b). In each figure the average result, shown as a heavy solid line, is obtained from three separate test observations shown as broken lines. The results of each test conducted within the entire study can be extracted from Supplementary Material S1.

For all tests, as summarised in Table 3, the load at first cracking σ_{cr} ranges 3.36–10.65 MPa (P_{cr} varied from 12.09 kN to 38.35 kN). The modulus of elasticities (E) also summarised in Table 3 and shows a variation from 14.99 GPa to 32.69 GPa where the average value at 30 days (16.23 GPa) is lower than that at 80 days specimen (30.19 GPa) and no significant increase with aging occurs beyond 80 days.

Following the formation of the crack, the tensile load is resisted by the fibres through the fibre-concrete bond, and in all cases strain hardening is observed (Fig. 4(b)), and where the magnitude of strain hardening stress (the difference in stress at the formation of the first crack and the stress at which the load starts to decrease) depends on the age of the concrete (varying between 19 % and 56 %).

In Fig. 4(a), although significant scatter is observed, there is a general increase in the strength and toughness with concrete age, and this behaviour can be attributed to an improvement in the fibre-concrete interfacial bond with concrete strength. Although the tensile response improves with concrete strength, as the fibres pull-out, at large crack-widths the responses become relatively independent of concrete strength, and this is because at large crack openings behaviour is controlled by friction between the fibre and the surrounding concrete and the embedded length of the individual fibres.

3.1.2. Corroded specimens

In this section, the effect of corrosion has been investigated by immersing the uncracked specimens in chloride solution for 4, 12, and 24 weeks (cw0-imm4, cw0-imm12, and cw0-imm24). The test results of these specimens under direct-tension are presented in the form of average σ-w plots in Fig. 5, which also include results of un-corroded specimens of similar ages (cw0-imm0–80d, cw0-

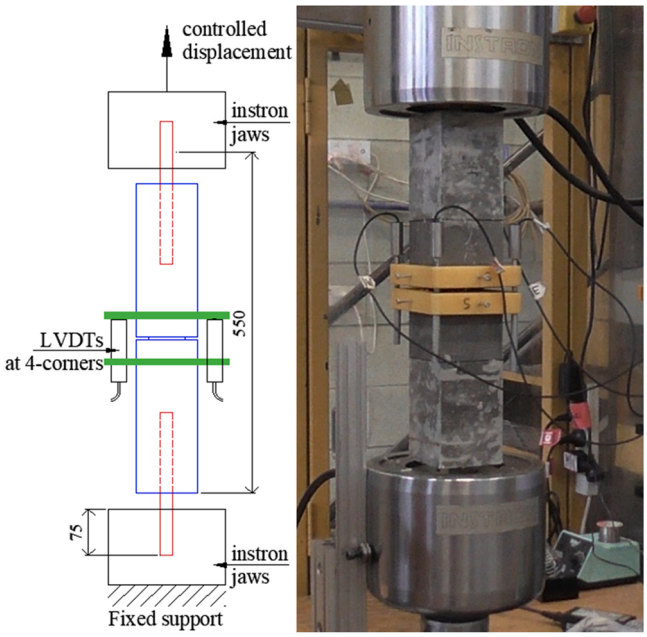

Fig. 3. Specimen dimension and direct-tension test set-up.

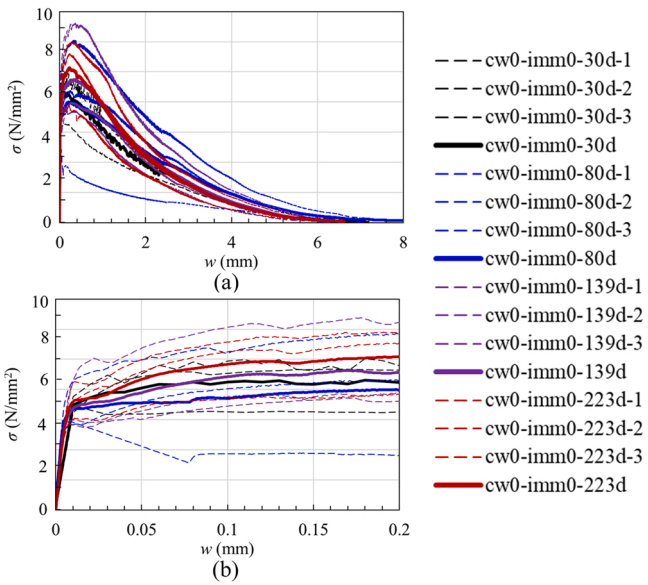

Fig. 4. σ-w of cw0-imm0.

imm0–139d, cw0-imm0–223d) as a benchmarking reference. It is to be noted that Fig. 5 presents the average response of three specimens for each category based on their age and corrosion level, and the individual test results are presented in Supplementary material S1. The figure also shows the results for different ranges of loading (Fig. 6(a): full range, Fig. 6(b): w is from 0 to 0.5 mm, Fig. 6 (c): w is from 0 to 0.05 mm) to highlight the important changes.

Comparing the results of the specimens that have been corroded to those that have not in Fig. 5, it can be seen that the strength at which cracking is initiated σ_{cr}, has significantly increased for corroded specimens (cw0-imm4, cw0-imm12, and cw0-imm24) in comparison to the corresponding un-corroded specimens (cw0-imm0–80d, cw0-imm0–139d, cw0-imm0–223d). Also of interest in Fig. 5(a) is that the difference between the σ-w response of corroded and un-corroded specimens is found to gradually reduce with increasing of crack opening and ultimately all responses converge.

The observed increase in strength shown in Fig. 5 can be explained by enhanced hydration of the cement and the associated pozzolanic reaction with the silica fume that occurs because of the increased availability of moisture [35,36]. For corroded specimens,

Table 3
Key stresses and corresponding crack widths (average of four corners) of corroded and un-corroded un-cracked specimens.

Specimen designation	Stress (N/mm^2)			Crack width (mm)			Elastic modulus (GPa), E
	σ_{cr}	$\sigma_1^{'}$	σ_{pk}	w_{cr}	$w_1^{'}$	w_{pk}	
cw0-imm0–30d-1	5.22	–	6.97	0.010	–	0.180	17.49
cw0-imm0–30d-2	4.48	–	6.47	0.010	–	0.150	14.99
cw0-imm0–30d-3	4.84	–	4.53	0.010	–	0.120	16.21
Avg. cw0-imm0–30d[a]	**4.84**	–	**5.99**	**0.010**	–	**0.150**	**16.23**
cw0-imm0–80d-1	3.39	–	6.04	0.004	–	0.261	28.39
cw0-imm0–80d-2	4.88	–	8.34	0.005	–	0.372	32.69
cw0-imm0–80d-3	3.52	–	2.61	0.004	–	0.141	29.48
Avg. cw0-imm0–80d	**3.93**	–	**5.66**	**0.004**	–	**0.258**	**30.19**
cw0-imm0–139d-1	3.88	–	5.16	0.005	–	0.172	25.99
cw0-imm0–139d-2	3.80	–	5.49	0.005	–	0.273	25.46
cw0-imm0–139d-3	4.24	–	9.14	0.006	–	0.373	23.67
Avg. cw0-imm0–139d	**3.97**	–	**6.60**	**0.005**	–	**0.273**	**25.04**
cw0-imm0–223d-1	3.37	–	7.73	0.004	–	0.233	28.22
cw0-imm0–223d-2	3.36	–	5.39	0.005	–	0.230	22.51
cw0-imm0–223d-3	4.59	–	8.28	0.006	–	0.269	25.63
Avg. cw0-imm0–223d	**3.77**	–	**7.13**	**0.005**	–	**0.244**	**25.45**
cw0-imm4–1	8.24	4.43	4.80	0.010	0.165	0.185	27.60
cw0-imm4–2	8.96	6.30	6.64	0.011	0.131	0.198	27.29
cw0-imm4–3	8.36	3.81	4.78	0.010	0.253	0.499	28.01
Avg. cw0-imm4	**8.52**	**4.85**	**5.41**	**0.010**	**0.183**	**0.294**	**27.63**
cw0-imm12–1	7.88	5.54	6.18	0.009	0.105	0.229	29.33
cw0-imm12–2	9.82	6.08	6.47	0.010	0.188	0.198	32.89
cw0-imm12–3	8.58	5.96	6.36	0.016	0.145	0.236	17.96
Avg. cw0-imm12	**8.76**	**5.86**	**6.34**	**0.012**	**0.146**	**0.221**	**26.73**
cw0-imm24–1	10.18	8.45	9.06	0.012	0.102	0.228	28.42
cw0-imm24–2	10.65	6.85	7.49	0.017	0.175	0.324	20.99
cw0-imm24–3	9.24	5.53	6.31	0.010	0.147	0.156	30.95
Avg. cw0-imm24	**10.02**	**6.94**	**7.62**	**0.013**	**0.141**	**0.236**	**26.79**

[a] Average of cw0-imm0–30d-1, cw0-imm0–30d-2 and cw0-imm0–30d-3

the load after the initial crack formation is observed to drop sharply to a stress $\sigma_1^{'}$ and gradually increases thereafter up to a peak stress σ_{pk}. The visible stress drops from σ_{cr} to $\sigma_1^{'}$ (strain softening) occurs because the load resisted by concrete prior to cracking cannot be resisted fully by the fibres at the initiation of cracking, and this behaviour is only seen to occur in specimens that have been immersed (corroded). These three critical stresses (σ_{cr}, $\sigma_1^{'}$, and σ_{pk}) and their corresponding crack openings are listed in Table 3 for all corroded and un-corroded specimens. The results summarised in Table 3 show that the post crack (initial) peak stress σ_{pk} of the corroded specimens is increased by between 32 % and 50 % of that of un-corroded specimens of similar age. This is due to a possible increase of bond strength that occurs with low levels of corrosion of un-cracked specimens. A similar finding is also observed by Yoo et al. [18] who reported that a low level of surface corrosion enhances bond performance due to surface roughness if the fibres pull-out completely without breaking.

Table 3 also presents the elastic modulus of corroded specimens (cw0-imm4, cw0-imm12, cw0-imm24). Significantly, when comparing the results of replicate tests, it can be observed that the scatter has increased in comparison to uncorroded specimens, it can also be seen that there is a wide variation (17.96–32.89 GPa) between that of the corroded and un-corroded specimens.

3.2. σ-w response of pre-cracked corroded specimens

The σ-w response of the 18 pre-cracked corroded specimens (3 durations of corrosion × 2 levels of pre-cracking × 3 specimens per case) are shown in Fig. 6, where the responses of individual specimens are shown with broken lines and the mean response of 3 specimens under each category are shown with solid lines. The full σ-w response in each case (Fig. 6) is comprised of 3 distinct stages, which are show schematically in Fig. 7. The first stage (o-a-b-c-d in Fig. 7) shows the response of an un-corroded specimen when loaded up to a predetermined stage in the post peak region corresponding to 15 % or 30 % drop of peak load; then fully unloaded with a residual crack width w_0. The second stage (d-e) represents the change of crack width from w_0 to $w_0^{'}$ during immersion of the specimens in chloride solution under no loading, and which is likely caused by self-healing of the cracked concrete.

The third stage (e-f-g in Fig. 7) shows the response of these corroded specimens when loaded again until their failure. For clarity of presentation, the experimentally derived σ-w response of these specimens is shown up to 2 mm crack-width (w) in Fig. 6, while full information for the entire range of loading is provided in the form of Supplementary Material S1. To benchmark the effect of immersion and corrosion, the σ-w response of un-corroded and uncracked (cw0-imm0) specimens of similar ages of ambient curing is also included in Fig. 6.

Under instantaneous loading conditions, if reloading is done immediately after unloading, the peak stress after reloading $\sigma_{pk\text{-}r}$ in Fig. 7 is expected to be close to σ_u, and the post-peak response of stage 3 will follow to the monotonically loaded response of the specimen beyond σ_u (Fig. 7). In this study, reloading is delayed by the immersion period, which can be expected to soften the response

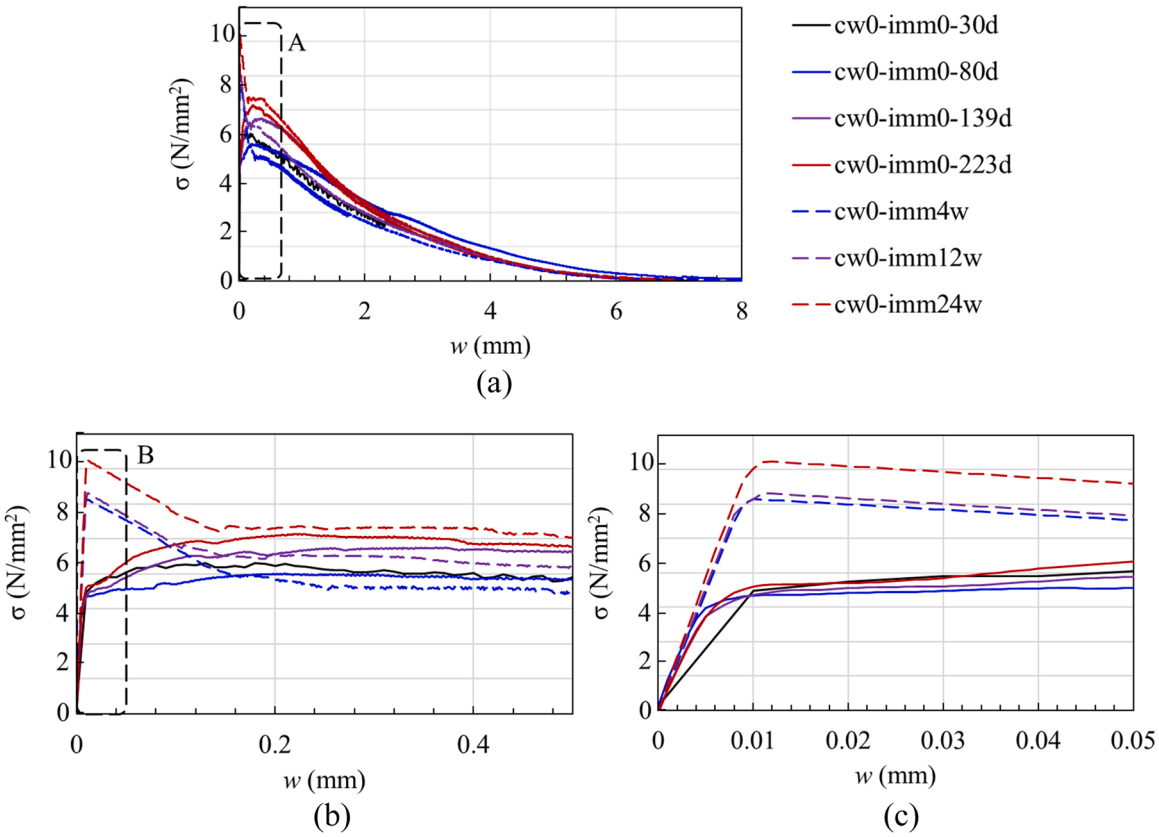

Fig. 5. Average σ-w response of corroded and un-corroded specimens (a) full range of loading, (b) w: 0–0.5 mm, marked A in Fig. 5(a), (c) w: 0–0.05 mm, marked B in Fig. 5(b).

through the mechanism of fibre corrosion and strengthen the response through self-healing, with the magnitude of change caused by each mechanism being a function of the level of pre-cracking and the period of immersion. Similar competing processes were identified Yoo et al. [17], but in this previous research multiple cracks were generated along the specimen length such that it was not possible to determine the influence of corrosion or self-healing at single location as is possible here.

In Fig. 6, the change in specimen strength and toughness due to corrosion can be considered in the stage 3 reloading response. This comparison can include the peak strength after reloading $\sigma_{pk\text{-}r}$ in comparison to the monotonic strength of the control specimens at the same crack width, and by considering the shape of the reloading curve until ultimate failure at point g in Fig. 7.

Taking specimen cw15-imm12–1 as a typical example, the stress corresponding to initiation of unloading (σ_u) has been found as 7.64 MPa while the peak stress for its reloaded region ($\sigma_{pk\text{-}r}$) has been found to be increased to 8.43 MPa (Table 4). This strength enhancement ($\sigma_{pk\text{-}r}$-σ_u) has been found to be similar to the remaining specimens in this category (12 weeks immersion and pre-cracking with $\sigma_u = 0.85\sigma_{pk}$ i.e., 15 % drop from σ_{pk}). For the same level of pre-cracking (cw15), the strength enhancement has been found to be more for 24 weeks immersion (cw15-imm24), and practically no enhancement/deterioration is observed for 4 weeks immersion (cw15-imm4). For the higher level of pre-cracking (cw30) with $\sigma_u = 0.70\sigma_{pk}$ (i.e., 30 % drop from σ_{pk}), $\sigma_{pk\text{-}r}$ has been found to be lower than σ_u (strength deterioration) for 4 weeks immersion, but the deterioration is reduced for 12 weeks immersion and enhanced for 24 weeks immersion. This clearly indicates that higher level of pre-cracking leads to strength deterioration, while longer immersion causes strength enhancement. A similar analysis can also be conducted using the values of the key parameters (σ_{pk}, σ_u, $\sigma_{pk\text{-}r}$, w_u, w_0, w_0') listed in Table 4.

Although competing mechanisms can be identified, in each set of experiments shown in Fig. 6, it can be seen that the residual strength following reloading lies within the scatter of the monotonic test results conducted at the same age. Although there is a very small quantity of data available, in an attempt to compare results, a student t-test (a standard statistical technique) is applied to compare $\sigma_{pk\text{-}r}$ with the stress of the corresponding uncracked but corroded specimen at the same crack-width. The outcome of this analysis shows that with 95% confidence (i.e., $p \leq 0.05$), the results from the two different test series can be considered to come from the same sample. This finding suggests that while pre-cracking resulted in the visual presence of corrosion (shown in Fig. 8), there was no significant change in mechanical response. A similar outcome was also observed by Yoo et al. [17] who found that the effect of corrosion on the fibre surface is overcome by self-healing due to formation of healing products ($CaCO_3$) that fills the cracks. Despite these initial findings, given the small number of test samples, further testing across a wide range of corrosion and pre-cracking levels is required to make more informed conclusions. It is further recommended that given that there was visual evidence of corrosion but that

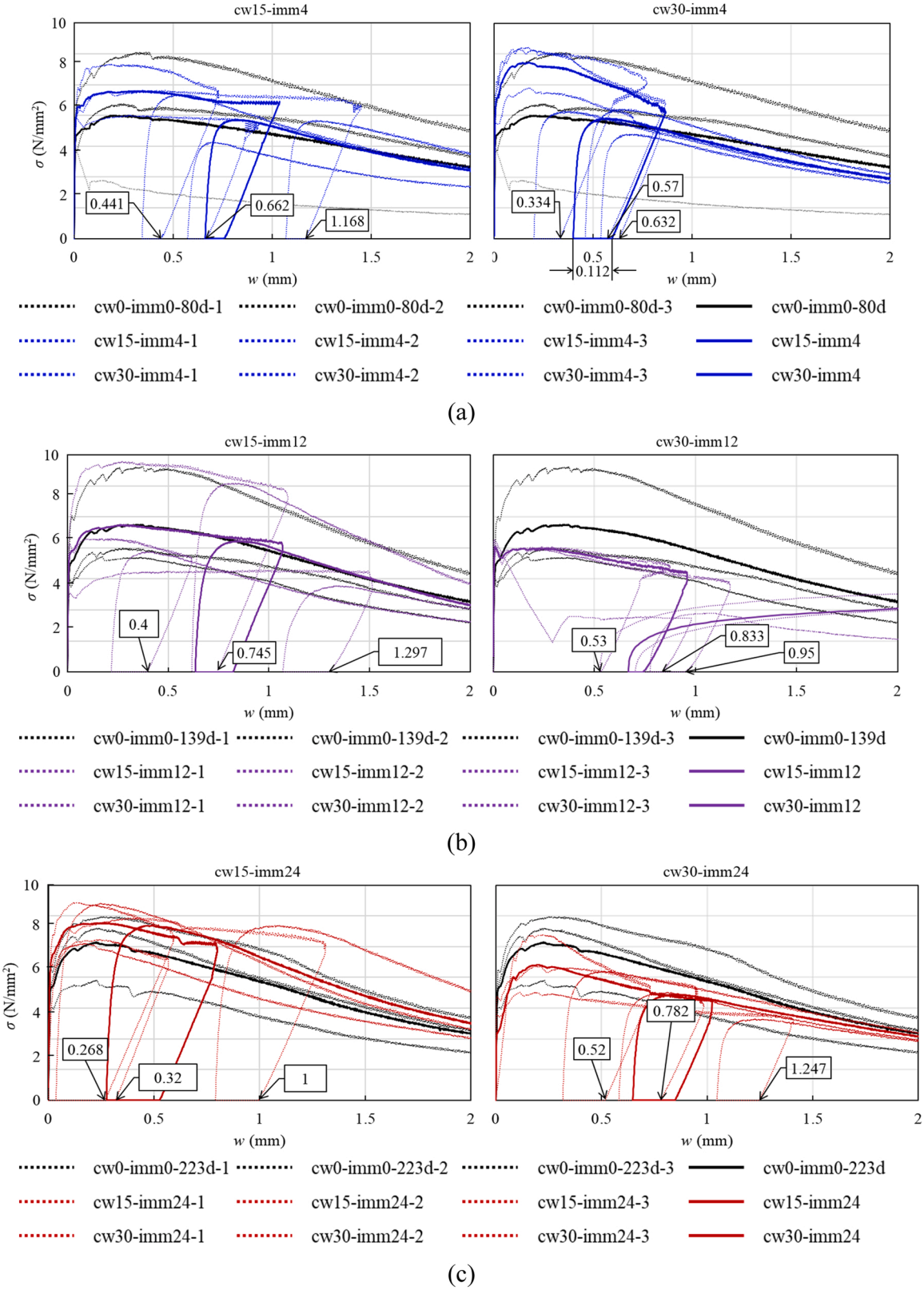

Fig. 6. *σ-w* response of pre-cracked corroded and uncracked un-corroded specimens.

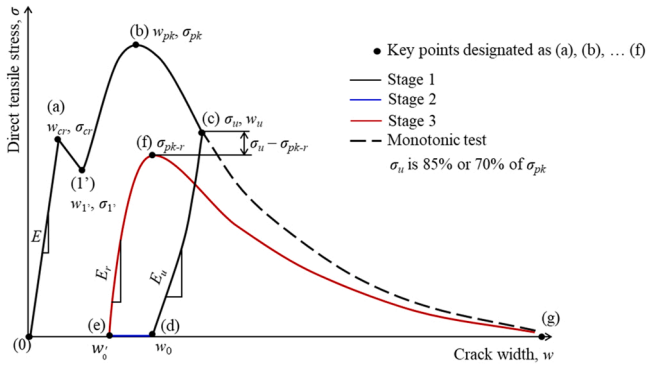

Fig. 7. Schematic diagram of stage 1 (up to d), stage 2 (d to e) and stage 3 (e to end) of the σ-w response.

Table 4
Important stresses, corresponding crack widths (average of four corners), and modulus of corroded and pre-cracked specimens.

	Stress (N/mm^2)				Crack width (mm)		Modulus (GPa)		
Specimen ID	σ_{pk}	σ_u	$\sigma_{pk\text{-}r}$	w_u	w_0	w_0'	E	E_u	E_r
cw15-imm4w-1	7.86	6.28	6.42	0.781	0.701	0.641	18.88	0.60	4.63
cw15-imm4w-2	6.67	5.40	5.24	1.412	1.352	1.254	32.66	0.74	4.57
cw15-imm4w-3	5.56	4.43	4.31	0.669	0.564	0.467	60.51	0.75	3.77
cw15-imm12w-1	9.42	7.64	8.43	0.746	0.699	0.573	31.29	0.74	7.28
cw15-imm12w-2	5.97	5.08	5.36	0.500	0.398	0.215	27.14	0.74	3.66
cw15-imm12w-3	4.56	3.62	3.80	1.061	0.951	0.723	97.71	0.57	2.23
cw15-imm24w-1	7.28	6.19	7.03	0.399	0.378	0.048	31.02	0.81	6.88
cw15-imm24w-2	8.94	7.42	8.87	0.324	0.294	0.061	18.43	0.74	6.63
cw15-imm24w-3	8.22	7.01	7.87	0.512	0.462	0.258	23.26	0.71	4.13
cw30-imm4w-1	6.81	4.57	4.68	0.658	0.592	0.499	49.53	0.74	6.20
cw30-imm4w-2	8.61	6.03	5.67	0.645	0.586	0.453	68.24	0.74	6.24
cw30-imm4w-3	8.50	5.95	5.84	0.651	0.541	0.430	29.14	0.67	5.82
cw30-imm12w-1	6.00	2.35	2.59	0.193	0.133	0.075	15.03	0.52	3.83
cw30-imm12w-2	5.90	3.83	2.68	0.810	0.733	0.514	27.73	0.65	3.87
cw30-imm12w-3	5.56	3.74	2.76	1.089	0.959	0.711	15.20	0.54	1.12
cw30-imm24w-1	4.89	3.28	3.63	0.325	0.220	0.200	25.50	0.72	5.16
cw30-imm24w-2	7.47	4.85	5.79	0.215	0.135	0.115	23.64	0.68	5.23
cw30-imm24w-3	6.06	4.24	4.85	0.195	0.195	0.176	26.25	0.60	4.61

Fig. 8. Corrosion of fibres (visual observation).

there was no significant change to the final σ/w response, that future tests must also consider approaches that can detail the spatial vitiation in corrosion.

Now considering the unloading and reloading response in more detail, in Table 4 the unloading modulus (E_u), reloading modulus (E_r), crack-width at zero load after unloading (w_0) and crack-width at zero load after conditioning (w'_0) are collated. It can be observed that the unloading modulus is significantly softer than that of the elastic modus of the uncracked concrete, and also of the concrete when reloading, and this is because the unloading modulus is related to the bond between the fibres and the concrete rather than the response of the concrete. In Table 4 it can also be observed that there is very little scatter between the unloading modulus, and this can

be expected because of similarity of ages of the specimens and the variation that is observed can be attributed to the variation of fibre volume and distribution between specimens. When considering the reloading modulus E_r, it can be seen to be significantly stiffer than that of the unloading branch and this may be attributed to the self-healing that occurred during immersion.

Although it is not the purpose of this paper to investigate the mechanisms or magnitude of self-healing in detail, it is possible to demonstrate that self-healing did occur via examining the change in crack-widths following immersion. To quantify this degree of self-healing, the crack closure in terms of reduction of crack width (w_0-$w_0^{'}$) has been presented in Table 4 for all immersed specimens. The microscopic image of the crack taken before and after immersion is shown in Fig. 9 for one of the specimens (cw30-imm24w-3) as a typical example at one of the predefined locations to have a visual representation of crack closure. Given the wide variation in crack-width measurements in Table 4, the results are summarised using a boxplot in Fig. 10, in which the percentage closure in crack width at each time period is presented for the low-crack specimens in part (a), and the high-crack specimens in part (b). In Fig. 10, the range, quartiles and median crack-width recovery is shown using a box plot, and the mean recovery is shown as a cross marker. Significantly, it can be observed that regardless of the initial crack width, after 24 months of exposure the mean crack recovery is above 80 % and the lower bound is above 50 %. The rate of crack recovery is however expected to be influenced by the initial crack width [37], geometrical properties of crack surface such as roughness, complexity, and continuity [38], fibre dispersion [39] and the presence of sustained or repeated loading. It is suggested here that further research is required under different exposure regimes to identify if this rate of recovery is achievable with exposure regimes that are similar to those seen in practice, i.e., wet and dry cycling versus continual exposure and also when specimens are subjected to a combination of mechanical and environmental loading.

4. Conclusions

The corrosion of ultra-high-performance fibre reinforced concrete has been investigated in this paper through the measurement of the stress-crack width response of corroded specimens. Significantly, this study has directly measured the stress-crack width response through the use of notched direct-tension specimens which have a sufficiently large cross-section to avoid preferential alignment of fibres. The effect of different levels of pre-cracking at a predefined locations and the duration of immersion (4, 12, and 24 weeks) in chloride solution have been investigated.

The key observations for this study are summarised below:

(1) The stress at the initiation of cracking varied within a range from 3.36 MPa to 10.65 MPa, and the elastic modulus varied between 14.99 GPa and 32.69 GPa. These variations are influenced by the concrete aging. However, the stiffness of concrete changed up to 80 days of age with no visible change beyond that, which indicates a matured state of the concrete.
(2) The stresses at the formation of the initial crack for corroded specimens with no pre-cracking has been found to be significantly higher than the post-cracking peak stress. This finding is opposite to what is observed in un-corroded specimens with no pre-cracking. The higher stress at crack initiation in corroded specimens can be explained by the enhanced hydration of binder and associated pozzolanic reaction with silica fume when specimens are immersed to induce corrosion. For corroded specimen with no pre-cracking, the bond strength increases due to increase of fibre surface roughness as a result of low levels of corrosion.
(3) The crack-width of pre-cracked specimens immersed in chloride solution has been found to reduce due to self-healing and on-going hydration. Some recovery of the stiffness degradation due to pre-cracking has also been observed due to self-healing. A general observation on the behaviour of all specimens indicates that a higher level of pre-cracking leads to strength deterioration while a longer period of immersion causes strength enhancement as the benefit of self-healing overcomes the deterioration caused by corrosion. This has been clearly observed pre-cracked specimens with longest period of immersion (24 weeks). Despite the degree of experimental scatter and the competing mechanisms of corrosion and self-healing, it is observed that following fibre corrosion the residual response of the specimens is similar to that of the control specimens.

Although here it has been shown that because of self-healing the response of the specimens following corrosion is similar to that of the control specimens, further detailed research is required to assess the impact of corrosion on self-healing and if this degree of self-healing would occur under realistic environmental and mechanical loading conditions. It is further necessary to understand the degree of spatial variation in fibre corrosion to identify if there is a size effect involved.

CRediT authorship contribution statement

Iftekhair Ibnul Bashar: Conceptualization, Formal analysis, Investigation, Writing – Original Draft; **Phillip Visintin:** Conceptualization, Methodology, Writing – Review & Editing, Supervision, Funding acquisition; **Abdul Hamid Sheikh:** Conceptualization,

(a) (b)

Fig. 9. (a) Crack before immersion, (b) healing of crack after 24 weeks immersion.

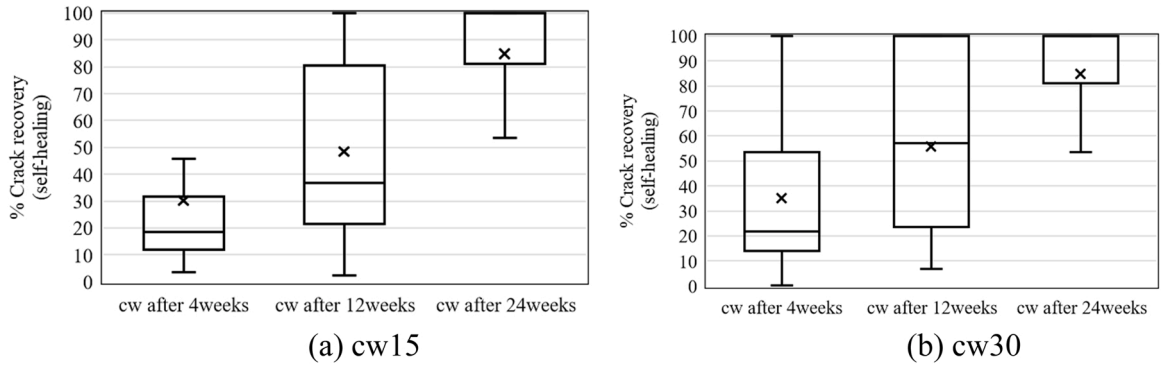

Fig. 10. Crack recovery (closure) over immersion ages of pre-cracked specimens.

Methodology, Writing – Review & Editing, Supervision.

Declaration of Competing Interest

The authors declare the following financial interests/personal relationships which may be considered as potential competing interests: Phillip Visintin reports financial support was provided by Australian Research Council.

Data availability

All data generated or used during the study appear in the published article, and Supplementary data S1.

Acknowledgements of funding

This material is based upon work supported by the Australian Research Council Discovery Project 190102650. First author acknowledges gratefully the Adelaide Scholarship International to facilitate this research work.

Appendix A. Supporting information

Supplementary data associated with this article can be found in the online version at doi:10.1016/j.cscm.2022.e01400.

References

[1] M. Singh, A.H. Sheikh, M.M. Ali, P. Visintin, M.C. Griffith, Experimental and numerical study of the flexural behaviour of ultra-high-performance fibre reinforced concrete beams, Const. Build. Mater. 138 (2017) 12–25, https://doi.org/10.1016/j.conbuildmat.2017.02.002.
[2] T. Xie, M.M. Ali, P. Visintin, Behaviour and analysis of ultra-high performance fibre reinforced concrete (UHPFRC) skew slabs, Eng. Struct. 199 (2019), 109588, https://doi.org/10.1016/j.engstruct.2019.109588.
[3] M. di Prisco, G. Plizzari, L. Vandewalle, Structural design according to fib MC 2010: comparison between RC and FRC elements, in: B. Massicotte, J. Charron, Plizzari, B. Mobasher, (eds), Proceedings of ACI-*fib* international workshop (ACI SP-310) on Fibre-reinforced concrete: From design to structural applications (fib CEB-FIP Bulletin 79), Montreal, Canada, 2016, pp. 69–87. American Concrete Institute Publications. ISBN 978–2-88394–119-9.
[4] C. Fang, M. Ali, T. Xie, P. Visintin, A.H. Sheikh, The influence of steel fibre properties on the shrinkage of ultra-high performance fibre reinforced concrete, Const. Build. Mater. 242 (2020), 117993, https://doi.org/10.1016/j.conbuildmat.2019.117993.
[5] T. Makita, E. Brühwiler, Tensile fatigue behaviour of ultra-high performance fibre reinforced concrete (UHPFRC), Mater. Struct. 47 (3) (2014) 475–491, https://doi.org/10.1617/s11527-013-0073-x.
[6] V. Marcos-Meson, A. Michel, A. Solgaard, G. Fischer, C. Edvardsen, T.L. Skovhus, Corrosion resistance of steel fibre reinforced concrete-A literature review, Cem. Concr. Res. 103 (2018) 1–20, https://doi.org/10.1016/j.cemconres.2017.05.016.
[7] Standards Australia, Concrete structures (AS3600:2018). Committee BD-002, Council of Standards Australia, 2018. ⟨https://www.standards.org.au/standards-catalogue/sa-snz/other/bd-002/as–3600-colon-2018⟩ (accessed 19 July 2022).
[8] H. Mihashi, S.F.U. Ahmed, A. Kobayakawa, Corrosion of reinforcing steel in fiber reinforced cementitious composites, J. Adv. Concr. Technol. 9 (2) (2011) 159–167, https://doi.org/10.3151/jact.9.159.
[9] T.T. Ngo, N.T. Tran, D.J. Kim, T.C. Pham, Effects of corrosion level and inhibitor on pullout behavior of deformed steel fiber embedded in high performance concrete, Const. Build. Mater. 280 (2021), 122449, https://doi.org/10.1016/j.conbuildmat.2021.122449.
[10] N.T. Tran, S. Pyo, D.J. Kim, Corrosion resistance of strain-hardening steel-fiber-reinforced cementitious composites, Cem. Concr. Compos. 63 (2015) 17–29, https://doi.org/10.1016/j.cemconcomp.2015.07.006.
[11] S.U. Balouch, J.P. Forth, J.L. Granju, Surface corrosion of steel fibre reinforced concrete, Cem. Concr. Res. 40 (3) (2010) 410–414, https://doi.org/10.1016/j.cemconres.2009.10.001.
[12] C.G. Berrocal, I. Löfgren, K. Lundgren, L. Tang, Corrosion initiation in cracked fibre reinforced concrete: influence of crack width, fibre type and loading conditions, Corros. Sci. 98 (2015) 128–139, https://doi.org/10.1016/j.corsci.2015.05.021.
[13] K. Hashimoto, T. Toyoda, H. Yokota, K. Kono, T. Kawaguchi, Tension-softening behavior and chloride ion diffusivity of cracked ultra-high strength fiber reinforced concrete, in: F. Toutlemonde, J. Resplendino (Eds), RILEM-*fib*-AFGC International Symposium on Ultra-High-Performance Fibre-Reinforced Concrete:

Designing and Building with UHPFRC, from Innovative to Large-scale Realizations: UHPFRC 2013, Marseille, France 2013, October 1-3, 2013, pp. 257–264. RILEM Publications ⟨https://www.rilem.net/publication/publication/422⟩ (accessed 19 July 2022).
[14] J.L. Granju, S.U. Balouch, Corrosion of steel fibre reinforced concrete from the cracks, Cem. Concr. Res. 35 (3) (2005) 572–577, https://doi.org/10.1016/j.cemconres.2004.06.032.
[15] S. Anandan, S.V.S. Manoharan, T. Sengottian, Corrosion effects on the strength properties of steel fibre reinforced concrete containing slag and corrosion inhibitor, Int. J. Corros. (2014), 595040, https://doi.org/10.1155/2014/595040.
[16] D.Y. Yoo, W. Shin, B. Chun, Corrosion effect on tensile behavior of ultra-high-performance concrete reinforced with straight steel fibers, Cem. Concr. Compos. 109 (2020), 103566, https://doi.org/10.1016/j.cemconcomp.2020.103566.
[17] D.Y. Yoo, W. Shin, B. Chun, N. Banthia, Assessment of steel fiber corrosion in self-healed ultra-high-performance fiber-reinforced concrete and its effect on tensile performance, Cem. Concr. Res. 133 (2020), 106091, https://doi.org/10.1016/j.cemconres.2020.106091.
[18] D.Y. Yoo, J.Y. Gim, B. Chun, Effects of rust layer and corrosion degree on the pullout behavior of steel fibers from ultra-high-performance concrete, J. Mater. Res. Technol. 9 (3) (2020) 3632–3648, https://doi.org/10.1016/j.jmrt.2020.01.101.
[19] D.Y. Yoo, W. Shin, Improvement of fiber corrosion resistance of ultra-high-performance concrete by means of crack width control and repair, Cem. Concr. Compos. 121 (2021), 104073, https://doi.org/10.1016/j.cemconcomp.2021.104073.
[20] E.F. O′Neil, J.T. Devlin, Durability of fiber-reinforced concrete under flexural stress in a severe marine environment, army engineer waterways experiment station Vicksburg MS Structures Lab, 1999. ⟨https://apps.dtic.mil/sti/citations/ADA369583⟩ (accessed 19 July 2022).
[21] B. Graybeal, J. Tanesi, Durability of an ultrahigh-performance concrete, J. Mater. Civ. Eng. 19 (10) (2007) 848–854, https://doi.org/10.1061/(ASCE)0899-1561(2007)19:10(848).
[22] A.G. Graeff, K. Pilakoutas, C. Lynsdale, K. Neocleous, Corrosion durability of recycled steel fibre reinforced concrete, Intersections. 6 (4) (2009) 77–79. ⟨http://www.intersections.tuiasi.ro/index.php/JIIR/article/view/539/524⟩ (accessed 19 July 2022).
[23] S. Abbas, A.M. Soliman, M.L. Nehdi, Exploring mechanical and durability properties of ultra-high-performance concrete incorporating various steel fiber lengths and dosages, Constr. Build. Mater. 75 (2015) 429–441, https://doi.org/10.1016/j.conbuildmat.2014.11.017.
[24] E. Alizade, A.F. Jandaghi, S. Zabihi, Effect of steel fiber corrosión on mechanical properties of steel fiber reinforced concrete, Asian J. Civ. Eng. 17 (2) (2016) 147–158. https://www.sid.ir/en/Journal/ViewPaper.aspx?ID=484640.
[25] J. Blunt, G. Jen, C.P. Ostertag, Enhancing corrosion resistance of reinforced concrete structures with hybrid fiber reinforced concrete, Corros. Sci. 92 (2015) 182–191, https://doi.org/10.1016/j.corsci.2014.12.003.
[26] J.P. Hwang, M.S. Jung, M. Kim, K.Y. Ann, Corrosion risk of steel fibre in concrete, Constr. Build. Mater. 101 (2015) 239–245, https://doi.org/10.1016/j.conbuildmat.2015.10.072.
[27] A. Masmoudi, J. Bouaziz, Durability of steel fibres reinforcement concrete beams in chloride environment combined with inhibitor, Adv. Mater. Sci. Eng. (2016), 1743952, https://doi.org/10.1155/2016/1743952.
[28] H. Sadeghi-Pouya, E. Ganjian, P. Claisse, K. Muthuramalingam, Corrosion durability of high-performance steel fibre reinforced concrete. In: Proceedings: SCMT3 Third International Conference on Sustainable Construction Materials and Technologies, Kyoto, Japan-August, (2013). ⟨https://iss.ndl.go.jp/books/R100000002-I024854037-00?ar=4e1f&locale=en⟩ (accessed 19 July 2022).
[29] A.K.H. Kwan, S.H. Chu, Direct tension behaviour of steel fibre reinforced concrete measured by a new test method, Eng. Struct. 176 (2018) 324–336, https://doi.org/10.1016/j.engstruct.2018.09.010.
[30] D. Dupont, L. Vandewalle, Distribution of steel fibres in rectangular sections, Cem. Conc. Compos. 27 (3) (2005) 391–398, https://doi.org/10.1016/j.cemconcomp.2004.03.005.
[31] S.J. Barnett, J.F. Lataste, T. Parry, S.G. Millard, M.N. Soutsos, Assessment of fibre orientation in ultra-high-performance fibre reinforced concrete and its effect on flexural strength, Mater. Struct. 43 (7) (2010) 1009–1023, https://doi.org/10.1617/s11527-009-9562-3.
[32] A.B. Sturm, P. Visintin, Local bond slip behavior of steel reinforcing bars embedded in ultra high performance fibre reinforced concrete, Struct. Concr. 20 (1) (2019) 108–122, https://doi.org/10.1002/suco.201700149.
[33] B.D. Sepulveda, P. Visintin, D.J. Oehlers, Quantifying the fatigue material properties of UHPFRC with steel microfibers at cracks, J. Struct. Eng. 147 (6) (2021), 04021076, https://doi.org/10.1061/(ASCE)ST.1943-541X.0003051.
[34] A.B. Sturm, P. Visintin, D.J. Oehlers, Mechanics of shear failure in fiber-reinforced concrete beams, J. Struct. Eng. 147 (3) (2021), 04020344, https://doi.org/10.1061/(ASCE)ST.1943-541X.0002934.
[35] P. Termkhajornkit, T. Nawa, K. Kurumisawa, Effect of water curing conditions on the hydration degree and compressive strengths of fly ash–cement paste, Cem. Concr. Compos. 28 (9) (2006) 781–789, https://doi.org/10.1016/j.cemconcomp.2006.05.018.
[36] Y. Senhadji, G. Escadeillas, M. Mouli, H. Khelafi, Influence of natural pozzolan, silica fume and limestone fine on strength, acid resistance and microstructure of mortar, Powder Technol. 254 (2014) 314–323, https://doi.org/10.1016/j.powtec.2014.01.046.
[37] D. Snoeck, N.De Belie, Mechanical and self-healing properties of cementitious composites reinforced with flax and cottonised flax, and compared with polyvinyl alcohol fibres, Biosyst. Eng. 111 (4) (2012) 325–335, https://doi.org/10.1016/j.biosystemseng.2011.12.005.
[38] T. Nishiwaki, M. Koda, M. Yamada, H. Mihashi, T. Kikuta, Experimental study on self-healing capability of FRCC using different types of synthetic fibers, J. Adv. Concr. Technol. 10 (6) (2012) 195–206, https://doi.org/10.3151/jact.10.195.
[39] E. Cuenca, L. Ferrara, Self-healing capacity of fiber reinforced cementitious composites. State of the art and perspectives, KSCE J. Civ. Eng. 21 (7) (2017) 2777–2789, https://doi.org/10.1007/s12205-017-0939-5.